Human Molecular Genetics, 2013, Vol. 22, No. 2 **203–217**
doi:10.1093/hmg/dds400
Advance Access published on October 3, 2012

Vacuolar-type H^+-ATPase V1A subunit is a molecular partner of Wolfram syndrome 1 (WFS1) protein, which regulates its expression and stability

Seley Gharanei[1,†], Malgorzata Zatyka[1,†], Dewi Astuti[1], Janine Fenton[1], Attila Sik[2,4], Zsuzsanna Nagy[3] and Timothy G. Barrett[1,*]

[1]Section of Medical and Molecular Genetics, [2]Neuroscience Networks Group, Neurobiology and Neuropharmacology, [3]Clinical and Experimental Medicine, School of Clinical and Experimental Medicine, College of Medical and Dental Sciences, University of Birmingham, Edgbaston, Birmingham B15 2TT, UK and [4]Department of Anatomy and Cell Biology, McGill University, Montreal, QC, Canada H3A 2B2

Received June 21, 2012; Revised and Accepted September 18, 2012

Wolfram syndrome is an autosomal recessive disorder characterized by neurodegeneration and diabetes mellitus. The gene responsible for the syndrome (*WFS1*) encodes an endoplasmic reticulum (ER)-resident transmembrane protein that also localizes to secretory granules in pancreatic beta cells. Although its precise functions are unknown, WFS1 protein deficiency affects the unfolded protein response, intracellular ion homeostasis, cell cycle progression and granular acidification. In this study, immunofluorescent and electron-microscopy analyses confirmed that WFS1 also localizes to secretory granules in human neuroblastoma cells. We demonstrated a novel interaction between WFS1 and the V1A subunit of the H^+ V-ATPase (proton pump) by co-immunoprecipitation in human embryonic kidney (HEK) 293 cells and with endogenous proteins in human neuroblastoma cells. We mapped the interaction to the WFS1-N terminal, but not the C-terminal domain. V1A subunit expression was reduced in *WFS1* stably and transiently depleted human neuroblastoma cells and depleted NT2 (human neuron-committed teratocarcinoma) cells. This reduced expression was not restored by adenoviral overexpression of BiP (immunoglobulin-binding protein) to correct the ER stress. Protein stability assays demonstrated that the V1A subunit was degraded more rapidly in WFS1 depleted neuroblastoma cells compared with wild-type; however, proteosomal inhibition did not restore the expression of the V1A subunit. Cell cycle assays measuring $p21^{cip}$ showed reduced levels in WFS1 depleted cells, and an inverse association between $p21^{cip}$ expression and apoptosis. We conclude that WFS1 has a specific interaction with the V1A subunit of H^+ ATPase; this interaction may be important both for pump assembly in the ER and for granular acidification.

INTRODUCTION

Neurodegeneration is a heterogeneous disorder characterized by the progressive loss of structure, function and death of neurons and is estimated to affect 1800 per 100 000 of the US population (1). Common contributing factors include genetic mutations, disorders of protein folding or protein degradation and disrupted apoptotic pathways.

Wolfram syndrome (WS) is a single gene neurodegenerative disorder mediated via endoplasmic reticulum (ER) stress and characterized by childhood onset diabetes mellitus, optic atrophy and motor, sensory and autonomic nervous system disruption (2). Many patients die prematurely with severe neurological disabilities such as central sleep apnoeas and organic brain syndrome (2). Imaging and post-mortem studies have shown diffuse neurodegenerative changes in the

*To whom correspondence should be addressed at: C/O Diabetes Unit, Birmingham Children's Hospital, Steelhouse Lane, Birmingham B4 6NH, UK. Tel: +1 1213339267; Fax: +1 1213339272; Email: t.g.barrett@bham.ac.uk
†The authors wish it to be known that, in their opinion, the first two authors should be regarded as joint First Authors.

brain (3). The causative gene, WFS1, was cloned in 1998 (4,5) and encodes an ER membrane protein, WFS1 protein or Wolframin (6), which contains nine transmembrane domains. Mice with disrupted WFS1 exhibit progressive pancreatic beta cell loss, resulting from the activation of ER stress pathways, delayed cell cycle progression and apoptosis (7–9). Wolframin expression is high in mouse and rat brains in the hippocampus cornu ammonis 1, amygdaloid areas, olfactory tubercles, cerebellum and superficial layer of the allocortex (10,11). This expression pattern correlates with the cerebellar ataxia, psychiatric and behavioural abnormalities seen in both humans and mouse models of WS (12–14).

Recently, it was shown that WFS1 plays a key role in the negative regulation of a feedback loop of the ER stress network through the ubiquitin proteasome pathway (15). We have previously shown that the Na^+/K^+ ATPase β1 subunit (ATP1B1) is a molecular partner of Wolframin, and WFS1 deficiency resulted in reduced expression of ATP1B1 (16). The mature sodium pump is located in the plasma membrane; however, during maturation, it is transiently present in the ER. Recently, it was shown that WFS1 is additionally located in the secretory granules of pancreatic beta cells and plays a role in granule acidification (17). Secretory granules are acidified through a proton gradient established and maintained by H^+ vacuolar-type ATPase (V-ATPase).

In this study, WFS1 depleted human neuroblastoma cells demonstrated increased ER stress response proteins. The WFS1 protein was found to localize to secretory granules in human neuroblastoma cells. These observations prompted us to investigate the possibility of an interaction between WFS1 protein and H^+ V-ATPase.

RESULTS

WFS1 depleted human neuronal cells demonstrate ER stress and apoptosis

We stably and transiently depleted *WFS1* in human neuroblastoma SK-N-AS and transiently depleted human neuronal NT2 (human neuron-committed teratocarcinoma) cells by short hairpin RNA (shRNA) and small interfering RNA (siRNA). Three *WFS1* stably depleted neuroblastoma clones (KD1–KD3) showed WFS1 expression significantly reduced by 60–80% in comparison with the control (CL) on both protein and RNA levels. *WFS1* transiently depleted cells showed 70–80% reduced expression in comparison with CL (Fig. 1A and B and Table 1; transiently depleted neuroblastoma and NT2 cell results, Supplementary Material, Fig. S1 and Table S1).

We measured the expression of ER stress markers in *WFS1* depleted neuroblastoma cells by a real-time polymerase chain reaction (PCR) and immunoblotting (Fig. 1, Table 1). The levels of the three ER stress markers CHOP [growth arrest and DNA-damage-inducible protein (C/EBP transcription factor)], BiP (immunoglobulin-binding protein) and spliced XBP1 were increased in both *WFS1* stably and transiently depleted neuroblastoma and NT2 cells in comparison with the CL on the RNA level (Fig. 1A; Table 1; Supplementary Material, Fig. S1A and C and Table S1) and the protein level (Fig. 1B and D; Table 1). The ER stress markers: ATF6a (activating transcription factor 6 alpha), and HRD1 (E3 ubiquitin-protein ligase synoviolin) were measured on the protein level, and their expressions were increased by 47–424% (Fig. 1C and D; Table 1). The levels of cleaved caspase-3 and pro-apoptotic protein CHOP were measured by immunoblotting: both were significantly increased in the three *WFS1* depleted clones in comparison to the control (1D). The expression of CHOP was increased by $95 \pm 15\%$, $96 \pm 62\%$ and $67 \pm 17\%$ in KD1-3 respectively, ($n = 3$ and $P < 0.05$). The expression of caspase-3 was increased by $73 \pm 18\%$, $100 \pm 41\%$, $47 \pm 6\%$ in KD1-3 respectively ($n = 5$, $P < 0.05$).

We also measured the levels of apoptosis in *WFS1* depleted neuroblastoma cells by High-Content Cytometry. The technique is based on detecting ongoing or early apoptosis by measuring total fluorescence from DNA fragmentation (18). The results are expressed as percentage apoptotic cells in the whole population. We demonstrated increased apoptosis in *WFS1* depleted neuroblastoma cells compared with CLs ($n = 5$, $P < 0.01$, Fig. 1E).

WFS1 localizes to the secretory vesicles in human neuroblastoma cell lines

It has been demonstrated that WFS1 localizes to the ER membrane (4,6,10). The study by Hatanaka *et al*. (17) reported co-localization between WFS1 and the secretory granule marker Chromogranin A in pancreatic beta cells. Therefore, we investigated whether WFS1 localizes to secretory vesicles in neuronal cells. V-ATPases are localized to secretory vesicles where they are involved in the acidification of secretory granules in both pancreatic and neuronal cells (17, 19, 20). Using immunofluorescence analysis, we showed the co-localization of WFS1 and VAMP (vesicle-associated membrane protein), and WFS1 and ATP6V1A (the V1A subunit of the proton pump), by confocal microscopy (Fig. 2A and B). We also confirmed WFS1 co-localization with an ER protein protein disulphide-isomerase (PDI; Fig. 2C). We then investigated the subcellular distribution of WFS1 in human neuroblastoma cells by electron microscopy (Fig. 2D–H). We observed a clear association of the WFS1 protein with the secretory vesicles (Fig. 2D). Silver intensified immunogold particles were absent in the nucleus (Fig. 2E, F and H) and mitochondria (Fig. 2H) and abundant in the cytoplasm.

The cytoplasmic domain (N-terminal) of WFS1 interacts with the V1A subunit of a proton pump

The possible association of WFS1 with ATP6V1A was investigated by co-immunoprecipitation (Co-IP) assays in transiently transfected HEK293 cells. We found that Myc-WFS1 interacts with FLAG-ATP6V1A (Fig. 3A and B). A 70 kDa protein was co-immunoprecipitated together with WFS1 (Fig. 3A, lane 3) using the anti-c-myc antibody, and the identity of this protein was confirmed as ATP6V1A by re-probing with a specific anti-ATPV1A antibody. In the reverse experiment, a 100 kDa protein was co-immunoprecipitated together with ATPV1A (Fig. 3B, lane 3) using the anti-FLAG antibody and was identified as a Wolfram protein by re-probing with a

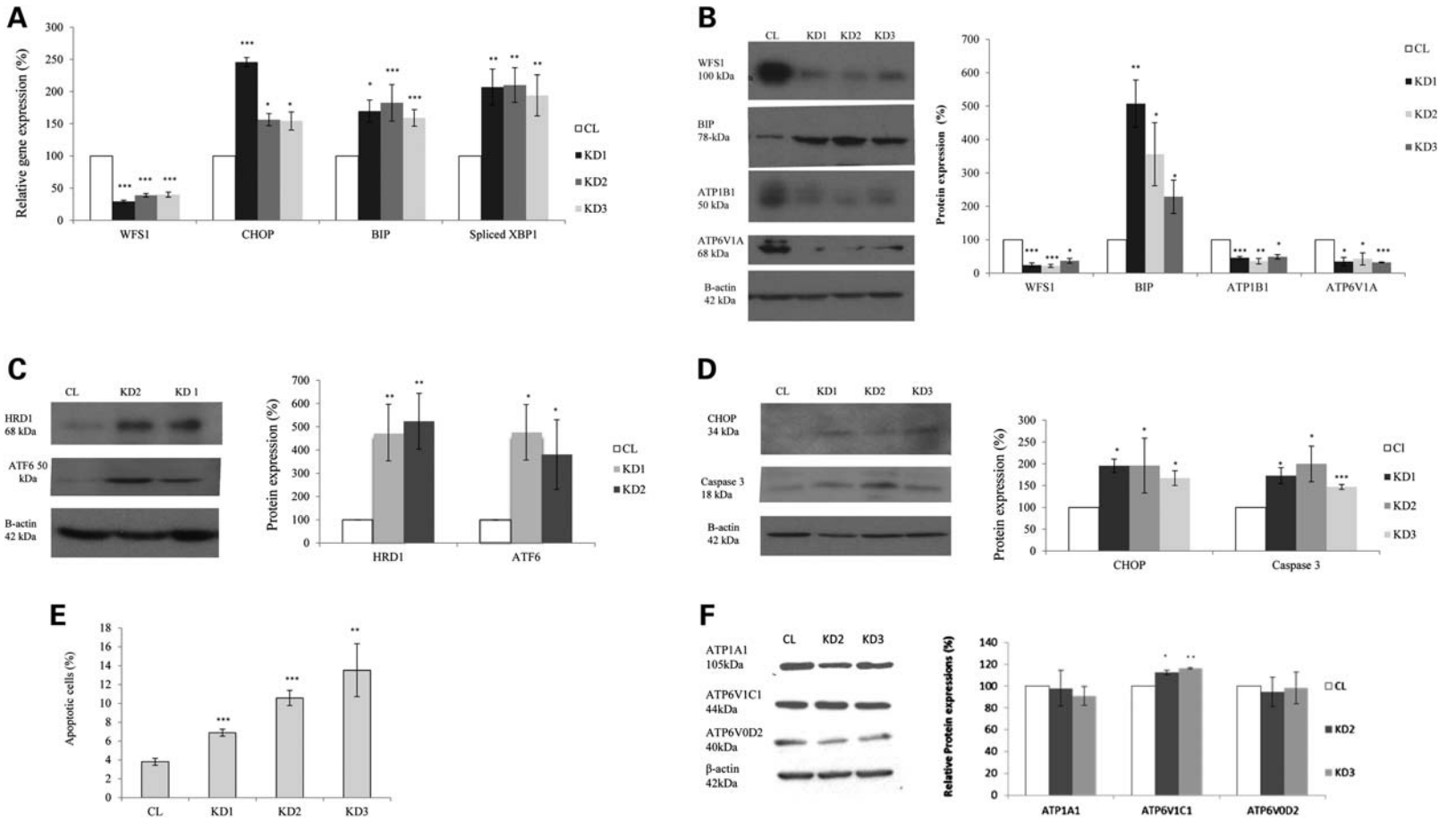

Figure 1. *WFS1* depletion in stable neuroblastoma clones results in the activation of ER stress response markers but decreased the expression of ATP1B1 and ATP6V1A. CL, control; KD1–KD3, WFS1 depleted stable clones. $^{*}P < 0.05$, $^{**}P < 0.01$ and $^{***}P < 0.001$. (**A**) QPCR analysis of *WFS1* and ER stress markers. *t*-test: WFS1 expression versus CLs: $P < 10^{-5}$ for KD1–KD3, $n = 6$; CHOP: $P < 10^{-5}$ for KD1 and $P < 0.05$ for KD2 and KD3, $n = 3$; BiP: $P < 0.05$ for KD1 and $P < 0.001$ for KD2 and KD3, $n = 5$; Spliced XBP1: $P < 0.01$ for KD1–KD3, $n = 7$ (n = number of independent runs using at least three RNA preparations from independently cultured stable clones). (**B**) Western blot analysis with antibodies to WFS1, BiP, ATP1B1 and ATP6V1A—representative experiment (β-actin = reference). Double bands may correspond to splice variants (at least two of ∼68 and 64 kDa are known). Bar chart—quantification of western blot, *t*-test versus CLs: WFS1: $P < 0.001$ for KD1 and KD2, $P < 0.05$ for KD3, $n = 6$; BIP: $P < 0.01$ for KD1 and $P < 0.05$ for KD2 and KD3, $n = 6$; ATP1B1: $P < 0.001$, $P < 0.01$ and $P < 0.05$ for KD1–KD3, respectively, $n = 6$; ATP6V1: $P < 0.05$ for KD1 and KD2 and $P < 0.001$ for KD3, $n = 3$ (n = number of independent runs using at least three independently prepared protein extracts). (**C**) Western blot analysis with antibodies to HRD1 and ATF6—representative immunoblot (β-actin = reference). Bar chart quantification of western blot: *t*-test versus CLs: HRD1: $P < 0.01$ for KD1 and KD2, $n = 4$; ATF6: $P < 0.05$ for KD1 and KD2, $n = 4$ (n = number of independent runs using three independently prepared protein extracts). (**D**) Western blot with antibodies to CHOP and cleaved caspase-3—representative immunoblot (β-actin = reference). Bar chart quantification of western blot, *t*-test versus CLs: CHOP: $P < 0.05$ for KD1, KD2 and KD3, $n = 3$; Caspase-3: $P < 0.05$ for KD1 and KD2 and $P < 0.001$ for KD3, $n = 5$ (n = number of independent runs using four independently prepared protein extracts). (**E**) Increase in the percentage of early apoptotic cells in the WFS1 depleted stable clones in comparison to the CL—High-Content Cytometry. *t*-test versus CLs: $P < 10^{-5}$ for KD1 and KD2 and $P < 0.01$ for KD3 versus CL, $n = 5$ [n = number of technical replicates (independent cultures of stable clones)]. (**F**) The expression levels of the α subunit of the sodium pump (ATP1A1) and ATP6V1C1 and ATP6V0D2 units of the proton pump do not depend on the presence of WFS1. Representative immunoblot with antibodies to ATP1A1, ATP6V1C1, ATP6V0D2 and β-actin. Immunoblot quantification: *t*-test: P = NS, $n = 3$ (n = number of protein extracts of stably WFS1 depleted neuroblastoma cells).

Table 1. Characterization of stable SK-N-AS clones with WFS1 depletion

Genes	KD1 (%)	KD2 (%)	KD3 (%)	Method	*n*	*P*-value
WFS1 depletion	71 ± 2	61 ± 3	60 ± 4	QPCR	6	<0.001
	76 ± 7	78 ± 4	63 ± 7	WB	6	<0.05
BiP induction	70 ± 17	83 ± 28	59 ± 13	QPCR	5	<0.05
	407 ± 71	255 ± 94	129 ± 49	WB	6	<0.05
CHOP induction	146 ± 7	56 ± 9	54 ± 14	QPCR	3	<0.05
	95 ± 15	96 ± 62	67 ± 17	WB	3	<0.05
Sp-XBP1 induction	107 ± 28,	110 ± 27	94 ± 33	QPCR	7	<0.01
ATF6a induction	377 ± 119	280 ± 149	NM	WB	4	<0.05
HRD1 induction	375 ± 121	424 ± 120	NM	WB	4	<0.05
Caspase-3 induction	73 ± 18	100 ± 41	47 ± 6	WB	5	<0.05
ATP6V1A reduction	66 ± 12	57 ± 18	67 ± 1	WB	3	<0.05
ATP1B1 reduction	54 ± 4	64 ± 8	51 ± 7	WB	6	<0.05

QPCR, real-time PCR; WB, western blotting; NM, not measured; NS, not significant; *n*, number of experiments; (%), fold change in comparison to the CL.

specific anti-WFS1 antibody. No Co-IP was observed in CL extracts co-transfected with either FLAG-empty/Myc-WFS1 or FLAG-V1A/Myc-empty plasmids (Fig. 3A and B, lanes 1 and 2). This interaction seems to be specific as we did not detect Co-IP between Myc-WFS1 and FLAG-RAS association domain family 1A or green fluorescent protein (GFP) (16) or between Myc-WFS1 and colipase, pancreatic lipase, regenerating protein or carboxypeptidase B1 (Prince S. and Zatyka M., unpublished data).

To test whether this interaction occurs with endogenously expressed proteins in human neuroblastoma SK-N-AS cells, an endogenous ATP6V1A protein was co-precipitated with WFS1 using the anti-WFS1 antibody (Fig. 3C, lane 2). No Co-IP was detected when the anti-FLAG antibody was used under the same conditions (Fig. 3C, lane 1), indicating that ATP6V1A interaction with the WFS1 antibody is specific. We concluded that the two proteins may associate *in vivo*.

The C-terminal domain of the WFS1 protein is located in the ER lumen and the N-terminal domain is located in the cytoplasm (21). To investigate the interacting domains of the WFS1 protein, Co-IP experiments were performed using constructs described previously (16). HEK293 cells were co-transfected with plasmids expressing either Myc-tagged N terminus of the Wolfram protein (amino acids 1–321) or the Myc-C-terminal domain of the Wolfram protein (amino acids 652–890) and FLAG-tagged ATP6V1A. For positive CL, HEK293 cells were co-transfected with plasmids expressing Myc-tagged full-length WFS1 and FLAG-tagged ATP6VIA. We found that there was an interaction of ATP6V1A with the cytoplasmic N-terminal domain of WFS1 (Fig. 3D, lane 3), whereas no interaction with the C-terminal domain of WFS1 (located in the ER lumen) was observed (Fig. 3E, lane 3). This suggests that the interaction between the Wolfram protein and the V1A subunit of the proton pump occurs in the cytoplasm.

WFS1 depletion is associated with decreased expression of the V1A subunit of the proton pump and the β1 subunit of Na^+/K^+ ATPase

After showing co-localization and interaction between WFS1 and ATP6V1A, we hypothesized that vesicular proton pump expression in neurons may be dependent on the presence of WFS1. Figure 1B and Table 1 show that the levels of the ATP6V1A protein were 57–67% decreased in *WFS1* stably depleted neuroblastoma clones in comparison with the CL. These findings were confirmed in both transiently WFS1 depleted models SK-N-AS and NT2 (Supplementary Material, Fig. S1B and D, panel 3, and Table S1).

We have previously shown an interaction between WFS1 and ATP1B1 and the decreased expression of ATP1B1 in WFS1 depleted MIN6 (mouse insulinoma pancreatic β cell line) cells and fibroblasts from patients with WFS1 mutations (16). Here, we found that the levels of ATP1B1 were also significantly decreased in *WFS1* depleted human neuronal cells. Figure 1B (3rd panel) and Table 1 show that the expression of ATP1B1 in *WFS1* stably depleted neuroblastoma cells was decreased by 51–64% in the knockdowns in comparison with the CL. The *WFS1* transiently depleted neuroblastoma cells and human NT2 cells also showed a significant reduction in the expression of ATP1B1 in comparison with the CL (Supplementary Material, Fig. S1B and D and Table S1). Our combined results suggest that *WFS1* may have a role in the expression and regulation of both sodium and proton pumps.

To determine whether *WFS1* depletion has an effect on other subunits of the relevant pumps, we measured the levels of ATP6V1C1 (the V1C1 subunit of the proton pump) and ATP6V0D2 subunits of the proton pump and the α subunit of the sodium pump (α-subunit of Na^+/K^+ ATPase, ATP1A1) in *WFS1* depleted and CL cells. The data presented in Figure 1F showed no significant decrease in the levels of expression on both ATP6V subunits, nor the α subunit of the sodium pump in *WFS1* depleted cells in comparison with the CL. These data suggest that the effect of WFS1 depletion could be specific for the β1 subunit of the sodium pump and the V1A subunit of the proton pump.

Correction of ER stress by adenoviral overexpression of BiP/glucose-regulated protein 78 has no effect on the expressions of the V1A subunit of the proton pump or the beta1 subunit of Na^+/K^+ ATPase

Adenoviral overexpression of the master ER stress chaperone BiP/GRP78 (glucose-regulated protein 78) has been used in many studies to reduce ER stress: For example, BiP

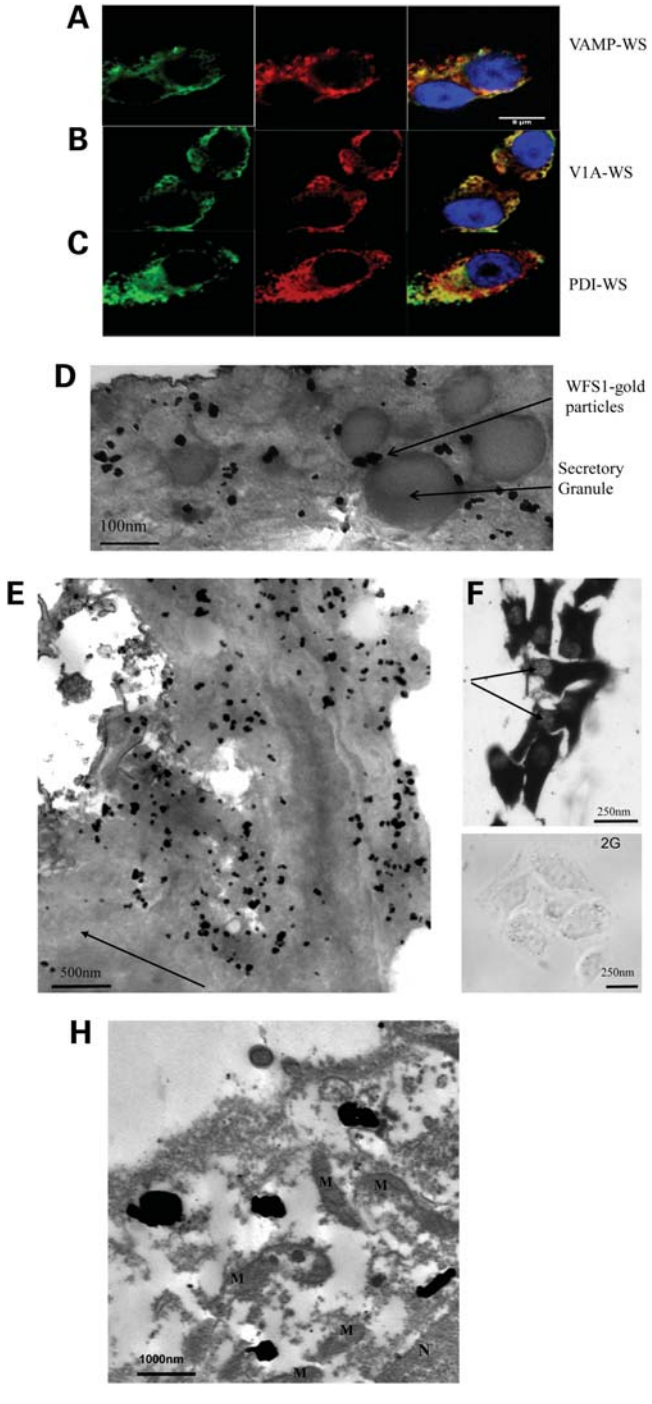

Figure 2. WFS1 localization in wild-type human neuroblastoma cell line SK-N-AS—confocal and electron microscopy. (**A**) Co-localization of WFS1 with VAMP (secretory vesicles)—immunofluorescence analysis using an antibody to WFS1 (green) and VAMP (red). (**B**) Co-localization of WFS1 with the V1A subunit of ATP6V1A (secretory vesicles)—immunofluorescence analysis using an antibody to WFS1 (green) and the V1A subunit of ATP6V1A (red). (**C**) Co-localization of WFS1 with PDI (ER)—immunofluorescence analysis using an antibody to WFS1 (green) and PDI (red). High resolution: 100× oil lens, scale bars represent 8 μm. (**D**) Representative electron micrograph showing the subcellular distribution of WFS1 in neuroblastoma cells and association with the secretory granules by pre-embedding immunogold staining. Scale bar represents 100 nm. (**E**) Enlarged field. Arrow points to the immunonegative nucleus visible in the bottom left corner. Scale bar represents 500 nm. (**F**) Light microscope picture of immunogold stained cells, arrows point to nuclei (lighter) lacking immunosignal. Scale bar 250 nm. (**G**) Negative CL (primary antibody omitted). Scale bar 250 nm. (**H**) Enlarged field. Letters signify mitochondria (M) and nucleus (N). Scale bar 1000nm.

overexpression attenuated increased CHOP expression and rescued cardiomyocytes from cell death (22). Similarly, the overexpression of BiP/GRP78 resulted in the normalization of the raised levels of PERK (protein kinase RNA-like endoplasmic reticulum kinase) phosphorylation in *WFS1*-deficient MIN6 cells (9). We therefore attempted to rescue ER stress in *WFS1* stably depleted neuroblastoma cells by infecting them with adenovirus overexpressing hamster BiP (ad.BiP) or a negative CL expressing GFP (ad.GFP). The adenovirus construct was a kind gift from Professor Guy Rutter (Imperial College London) and was amplified and purified using CsCl (caesium chloride) banding. BiP expression measured by a real-time PCR was ∼2-fold higher in ad.BiP-infected cells in comparison with ad.GFP-infected cells (Fig. 4A) with the fold-changes 169 ± 20, 241 ± 8, 197 ± 20 and $204 \pm 30\%$ in CL and KD1–KD3, respectively ($n = 3$, $P < 0.05$). Significant increases in BiP protein levels were demonstrated in ad.BiP-infected cells: 1569 ± 459, 1292 ± 296, 1430 ± 664 and 960 ± 107 in CL and KD1–KD3, respectively ($n > 3$, $P < 0.05$, Fig. 4B).

Next, we measured the levels of ER stress markers in ad.BiP-infected cells relative to ad.GFP-infected cells (the expression of each of the markers in the ad.GFP-infected clones was assigned as 100%). As shown in Fig. 4C, CHOP mRNA was decreased to 87 ± 4, 71 ± 17, 89 ± 7 and $83 \pm 5\%$ in CL and KD1–KD3, respectively, in ad.BiP-infected cells in comparison with ad.GFP-infected cells ($n = 3$, $P < 0.05$). The expression of spliced XBP1 was decreased to 68 ± 8, 64 ± 19, 47 ± 5 and $70 \pm 8\%$ in CL, KD1, KD3, respectively, in ad.BiP-infected samples in comparison with the ad.GFP-infected cells ($n = 3$, $P < 0.05$). Glucose regulating protein 94 (GRP94) mRNA levels in ad.BiP-treated cells were decreased to 65 ± 17, 48 ± 15, 73 ± 2 and $70 \pm 15\%$ in CL and KD1–KD3, respectively ($n = 3$, $P < 0.05$). The largest decrease was measured for endogenous BiP with decrease to 19 ± 18, 10 ± 8, 35 ± 16 and $26 \pm 11\%$ in ad.BiP- versus ad.GFP-infected CL and KD1–KD3, respectively ($n = 3$, $P < 0.05$).

The expression of GRP94 was also measured by immunoblotting (Fig. 4D). GRP94 expression was decreased in ad.BiP-infected cells to 56 ± 10, 70 ± 13, 64 ± 10 and $80 \pm 3\%$ in CL and KD1–KD3, respectively, relative to ad.GFP-infected cells ($n = 3$, $P < 0.05$; the protein levels in ad.GFP-infected cells were assigned as 100%). To evaluate the effect of ad.BiP overexpression on apoptosis, we measured apoptotic cells by High-Content Cytometry; the data presented in Fig. 4E and Table 2 show that, within each cell line, the number of apoptotic cells was significantly reduced in ad.BiP-infected cells in comparison with the ad.GFP infection. The apoptosis noted in the CL GFP-infected cells is likely to be that induced by the experimental procedure rather than the 'baseline' rate of apoptosis in these cells. In summary, we

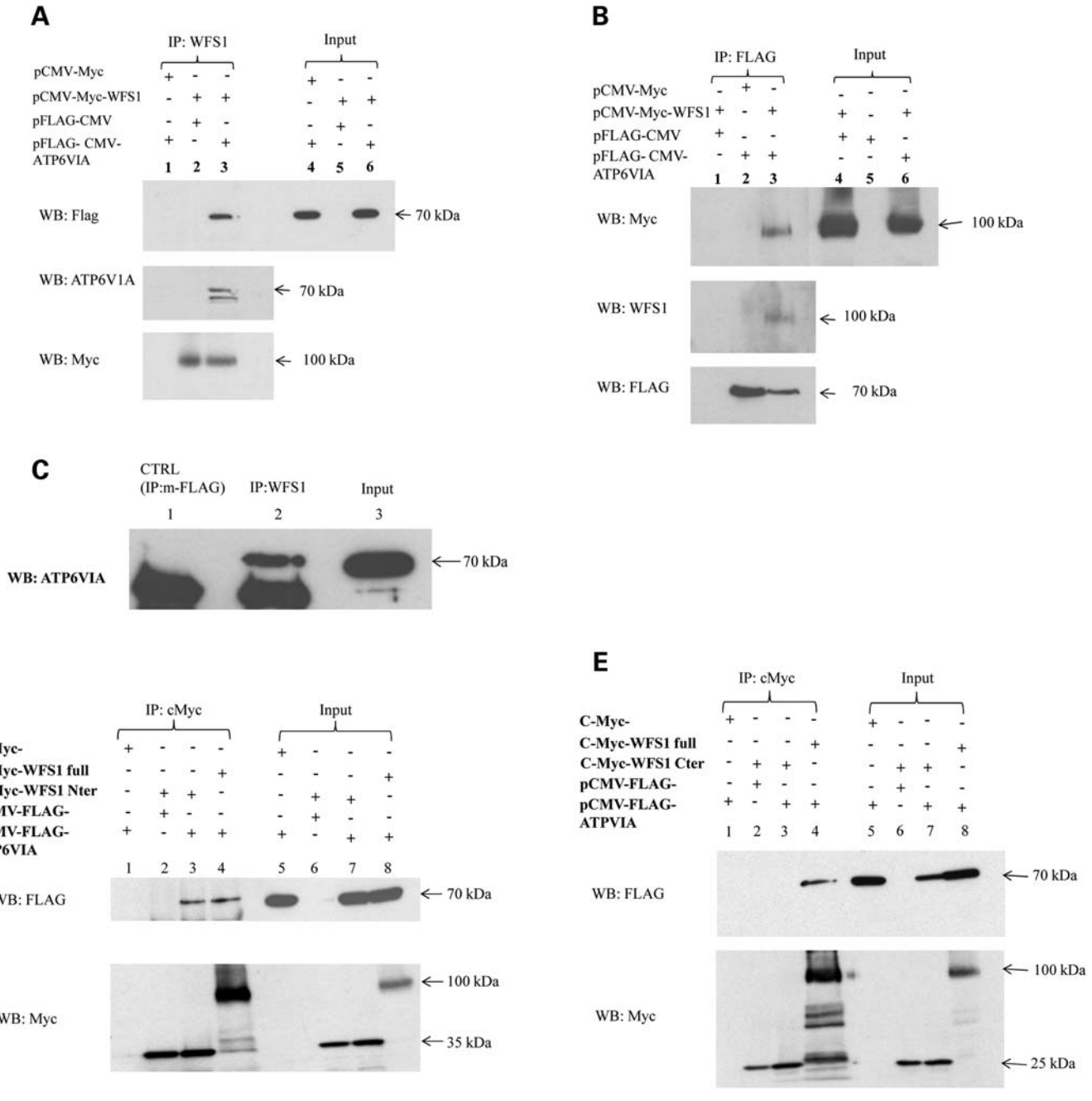

Figure 3. Interaction of WFS1 with the V1A subunit of the proton pump. (**A**) Co-IP of full-length c-myc-tagged WFS1 with the FLAG-tagged V1A subunit of the proton pump co-trasfected with HEK293 cells, using the rabbit polyclonal WFS1 antibody (lanes 1–3). The mouse monoclonal FLAG antibody was used for detection. The identity of the detected protein was confirmed by re-probing with a specific antibody to anti-ATP6V1A (mouse monoclonal). Double bands may correspond to splice variants (at least two, of ~68 and 64 kDa are known). Bottom panel: re-probing with the c-myc antibody (mouse monoclonal) shows the presence of WFS1 in the relevant extracts (lanes 2 and 3); input (4% of total extracts used for IP). (**B**) Co-IP of full-length c-myc-tagged WFS1 and the FLAG-tagged V1A subunit with the mouse monoclonal FLAG antibody (lanes 1–3). Detection with the polyclonal, rabbit c-myc antibody and (below) re-probing with the anti-WFS1 antibody (rabbit polyclonal) to confirm the identity of the co-precipitated protein. (Bottom panel) Re-probing with polyclonal rabbit FLAG antibodies to demonstrate the presence of V1A in relevant extracts (lanes 2 and 3). Input: 4% of total lysates used for IP. (**C**) Interaction between endogenous proteins (WFS1 and V1A) in human neuroblastoma cells. Rabbit polyclonal anti-WFS1 antibody was used for co-precipitation and mouse monoclonal anti-V1A antibodies were used for immunoblotting (lane 2). Negative CL: pull down with the FLAG antibody (mouse monoclonal, lane 1). Input (lane 3): 2% of total lysates used for IP. (**D**) The N-terminal domain of WFS1 interacts with ATP6V1A. Co-IP of the c-myc-tagged N-terminal domain of WFS1 (amino acids 1–321) with FLAG-tagged ATP6V1A with the c-myc rabbit polyclonal antibody in HEK293 cells (lanes 1–3). Detection: with mouse monoclonal FLAG antibodies. Full-length myc-WFS1 was used as a positive CL for interaction (lane 4). Bottom panel: re-probing with c-myc (mouse monoclonal antibody) to demonstrate the presence of either truncated (lanes 2 and 3) or full-length (lane 4) WFS1. Input: 4% of total lysates used for IP. (**E**) The C-terminal domain of WFS1 does not interact with ATP6V1A. There is no Co-IP of the c-myc-tagged C-terminal domain (amino acids 652–890) of WFS1 with FLAG-tagged ATP6V1A with the c-myc rabbit polyclonal antibody in HEK293 cells (lanes 1–3). Immunoblotting: with mouse monoclonal FLAG antibodies. Full-length c-myc WFS1 was used as a positive CL for interaction (lane 4). Bottom panel: re-probing with c-myc (mouse monoclonal) to demonstrate the presence of either full-length (lane 4) or truncated (lanes 2 and 3) WFS1. Input: 4% of total lysate used for IP.

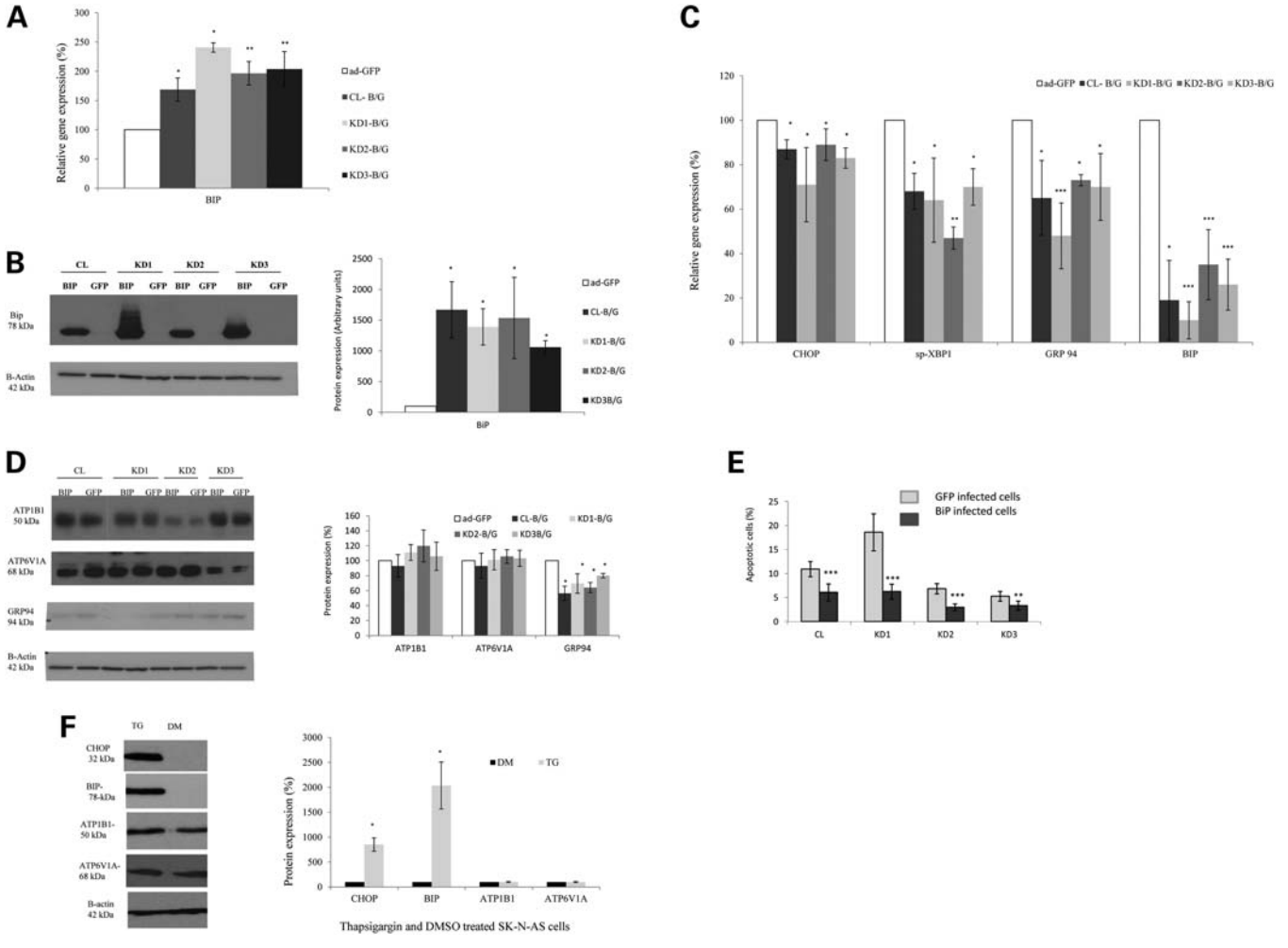

Figure 4. Adenoviral overexpression of GRP78/BiP in WFS1 stably depleted neuroblastoma cells. After 24 h of growing, the cells were infected with either ad.BiP or ad.GFP at MOI = 8.5, 16 h later harvested for either RNA or protein analysis. CL, control; KD1, KD2 and KD3 stably WFS1 depleted clones. $^{*}P < 0.05$, $^{**}P < 0.01$ and $^{***}P < 0.001$. (**A**) The overexpression of BiP mRNA in stably depleted clones infected with ad.BiP in comparison with corresponding CLs infected with ad.GFP. The expression of BiP was assumed equal to 100% for each ad.GFP-infected clones (CL and KD1–KD3) and is illustrated by one white bar on the chart. QPCR analysis, *t*-test: ad.BiP CL/ad.GFP CL and ad.BiP KD1/ad.GFP KD1, $P < 0.05$; ad.BiP KD2/ad.GFP KD2 and ad.BiP KD3/ad.GFP KD3, $P < 0.01$ ($n = 3$). (**B**) The overexpression of the BiP protein—representative immunoblot with an antibody to BiP and β-actin. Bar chart: immunoblot quantification: the expression of BiP was assumed equal to 100 arbitrary units for each ad.GFP-infected clone (CL and KD1–KD3) and is illustrated by one white bar on the chart. *t*-test ad.BiP/ad.GFP for all clones was $P < 0.05$. The expression of BiP is presented in arbitrary units. Ad.GFP-infected clones (CL and KD1–KD3) are illustrated by one white bar on the chart. (**C**) QPCR analysis of the expression of ER stress markers in stably depleted clones infected with ad.BiP in comparison with the corresponding CLs infected with ad.GFP. The expression of each marker was assumed equal to 100% for each ad.GFP-infected clone (CL and KD1–KD3) and is illustrated by one white bar on the chart. *t*-test: CHOP ad.BiP/ad.GFP for the CL and depleted cell lines was $P < 0.05$. Spliced XBP1: $P < 0.05$ for ad.BiP CL/ad.GFP CL, ad.BiP KD1/ad.GFP KD1 and ad.BiP KD3/ad.GFP KD3; for ad.BiP KD2/ad.GFP KD2, $P < 0.01$. GRP94: $P < 0.05$ for ad.BiP CL/ad.GFP CL, ad.BiP KD2/ad.GFP KD2 and ad.BiP KD3/ad.GFP KD3; $P < 0.001$ for ad.BiP KD1/ad.GFP KD1. Endogenous BiP: $P < 0.05$ for ad.BiP CL/ad.GFP CL; $P < 10^{-5}$ for ad.BiP KD1/ad.GFP KD1 and ad.BiP KD3/ad.GFP KD3; $P < 0.001$ for ad.BiP KD2/ad.GFP KD2. ($n = 3$ in all experiments). (**D**) Representative immunoblot with antibodies to ATP1B1, ATP6V1A, GRP94, β-actin and immunoblot quantification in stably *WFS1* depleted clones infected with ad.BiP in comparison with corresponding CLs infected with ad.GFP. The expression of each protein was assumed equal to 100% for each ad.GFP-infected clone (CL and KD1–KD3) and is illustrated by one white bar on the chart. *t*-test for ATP1B1 and ATP6V1A: P = NS for all clones ($n = 3$). GRP94: ad.BiP/ad.GFP $P < 0.05$ for all clones ($n = 3$). ATP1B1 expression was measured as 93 ± 15, 111 ± 11, 120 ± 21 and $106 \pm 19\%$ in CL and KD1–KD3, respectively. The ATP6V1A expression in ad.BiP-infected versus ad.GFP-infected samples showed 93 ± 17, 101 ± 13, 105 ± 9 and $103 \pm 11\%$ in CL and KD1–KD3, respectively. (**E**) Reduction in the number of apoptotic cells in WFS1 depleted stable clones after the adenoviral transduction of BiP in comparison with cells transduced with ad.GFP ($P < 0.01$). GFP-infected, BiP-infected [CL = 11 ± 1.6, 6 ± 1.7 ($P < 0.001$)], KD1 [19 ± 3.9, 6 ± 1.6 ($P < 0.001$)], KD2 [7 ± 1, 3 ± 1 ($P < 0.001$)] and KD3 [5 ± 1, 3 ± 1 ($P < 0.001$)]. (**F**) Chemical induction of ER stress in wild-type SK-N-AS cells—representative immunoblot with antibodies to CHOP, BiP, ATP1B1, ATP6V1A and β-actin. Neuroblastoma cells were treated with 1 μM TG for 24 h before harvesting in RIPA buffer (TG, thapsigargin; DM, DMSO). Immunoblot quantification: *t*-test: CHOP and BiP, $P < 0.05$; ATP1B1 and ATP6V1A, P = NS.

abolished the enhanced ER stress response and demonstrated a reduction in the levels of ER stress markers and apoptotic cells by the adenoviral overexpression of BiP/GRP78.

Next, we evaluated whether the overexpression of BiP affects the expression levels of ATP6V1A and ATP1B1 proteins. The results presented in Fig. 4D shows no significant

Table 2. Cell cycle and apoptosis data of WFS1 depleted neuroblastoma cells

Measured parameters	CL	KD1	KD2	KD3
G1 cells (%) at 24 h	56 ± 0.3	77 ± 1.3	55 ± 0.4	44 ± 0.4
G2 cells (%) at 24 h	29 ± 0.3	12 ± 0.4	30 ± 0.5	35 ± 0.5
G1 cells (%) at 48 h	47 ± 0.3	68 ± 0.4	32 ± 0.5	47 ± 0.3
G2 cells (%) at 48 h	36 ± 0.4	18 ± 0.4	48 ± 0.8	32 ± 0.6
PDT (h)	65 ± 2	65 ± 3	54 ± 3	65 ± 2
G1 time (h)	25 ± 0.8	39 ± 1.5	14 ± 0.7	25 ± 0.8
G2 time (h)	29 ± 1	16 ± 1	31 ± 2	26 ± 1
Ad-BiP-apop cells (%)	6 ± 1.7	6 ± 1.6	3 ± 1	3 ± 1
Ad-GFP-apop cells (%)	11 ± 1.6	19 ± 3.9	7 ± 1	5 ± 1
Ad-BiP-G1 cells	16 ± 6.2	9 ± 2.6	12 ± 4	11 ± 3
Ad-GFP-G1 cells	41 ± 2.6	52 ± 3.5	25 ± 2	22 ± 3
P21-protein per cell	303 ± 43	226 ± 42	243 ± 18	89 ± 12
P21-pos-G2 cells (%)	44 ± 2.6	34 ± 3.8	67 ± 4.5	65 ± 10.7
P21-neg-G2 cells (%)	13 ± 1.9	6 ± 1.2	8 ± 2.3	29 ± 3.9
P21-pos-apop cells	1 ± 0.3	1 ± 0.4	0 ± 0.3	1 ± 0.4
P21-neg-apop cells	19 ± 3	20 ± 3	23 ± 0.3	9 ± 3.1

PDT, population doubling time; apop, apoptosis; h, hours; %, cells in cells cycle phase; Ad-GFP-apop cells, adenoviral-BiP transfected cells showing apoptosis; Ad-BiP-G1 cells, adenoviral-BiP transfected cells in the G1 phase; Ad-GFP-apop cells, adenoviral-GFP transfected cells showing apoptosis; P21-pos-G2 cells, cells expressing $p21^{cip}$ in the G2 phase.

difference in the expression of both proteins in ad.BiP-infected cells relative to ad.GFP-infected cells. Furthermore, the chemical induction of ER stress was undertaken to evaluate whether the expression of ATP6V1A and ATP1B1 were sensitive to ER stress. Wild-type SK-N-AS cells were treated with 1 μM thapsigargin for 24 h, and the expressions of ATP6V1A, ATP1B1 and ER stress markers BiP and CHOP were measured by immunoblotting. As shown in Fig. 4F, thapsigargin treatment resulted in the expected elevation of BiP and CHOP expression by 753 ± 134 and 1936 ± 471%, respectively ($n = 3$, $P < 0.05$). On the contrary, both ATP6V1A and ATP1B1 were expressed at similar levels in thapsigargin-treated cells and dimethyl sulfoxide (DMSO)-treated CL. ATP6V1A expression was 100 ± 10% in thapsigargin-treated samples and ATP1B1 expression was 102 ± 10% versus DMSO-treated cells ($n = 4$, $P =$ NS).

Our results show that ER stress measured as elevated levels of CHOP, BIP, spliced XBP1 and GRP94 in *WFS1* depleted neuroblastoma cells was reduced by the overexpression of hamster BiP resulting in the abolition of the previously observed enhanced ER stress response. The overexpression of hamster BiP did not affect the expression of ATP6V1A or ATP1B1, and the experiment with thapsigargin did not show any dependence of ATP6V1A or ATP1B1 expression on ER stress levels.

WFS1 is involved in the stability of proton and sodium pump subunits

We next hypothesized that *WFS1* may be necessary for the stability of ATP6V1A and ATP1B1. To investigate this hypothesis, we undertook protein stability assays in which the degradation rate of ATP6V1A or ATP1B1 subunits in *WFS1* depleted cells was compared with wild-type CL. *WFS1* stably depleted neuroblastoma cells were treated with a protein translation inhibitor (cycloheximide, CX) at a concentration of 50 μg/ml and harvested in radioimmunoprecipitation assay (RIPA) buffer for immunoblotting at 2 h intervals over 6 h. The toxicity assay showed that treatment with up to 90 μg/ml of CX for 24 h was not toxic to neuroblastoma cells (data not shown).

In *WFS1* depleted cells, ATP6V1A was more rapidly degraded in comparison with the CL, in which ATP6V1A expression was stable over a 6 h time course and showed 101 ± 22% at the end of the experiment in comparison with time 0 ($n = 3$, $P =$ NS, Fig. 5A). Two hours after CX treatment, there was 75 ± 2% ($P = 0.001$) of ATP6V1A remaining in KD1, 57 ± 9% ($P = 0.01$) in KD2 and 67 ± 13% ($P = 0.03$) in KD3 in comparison with time 0. At 4 h, there was 42 ± 3% ($P = 2 \times 10^{-4}$) of ATP6V1A remaining in KD1, 43 ± 13% ($P = 0.005$) in KD2 and 63 ± 12% ($P = 0.035$) in KD3, whereas after 6 h treatment, there was only 18 ± 2% ($P < 4 \times 10^{-5}$) in KD1, 30 ± 11% ($P = 0.005$) in KD2 and 49 ± 3% ($P = 2 \times 10^{-4}$) in KD3 in comparison with time 0 ($n = 4$).

Similarly in *WFS1* depleted cells, ATP1B1 was more rapidly degraded in comparison with the CL, where ATP1B1 seemed to be stable over a 6 h time course (the 15% decrease after 6 h was not statistically significant, Fig. 5B). Two hours after CX treatment, there was only 70 ± 9% ($P = 1.9 \times 10^{-4}$) of ATP1B1 remaining in KD1, 83 ± 8% ($P = 0.018$) in KD2 and 93 ± 2% ($P = 0.016$) in KD3 in comparison with time 0. Four hours after CX treatment, there was only 56 ± 9% ($P = 3.5 \times 10^{-4}$) of ATP1B1 remaining in KD1, 47 ± 13% ($P = 0.018$) in KD2 and 71 ± 4% ($P = 0.016$) in KD3. Finally, after 6 h of CX treatment, there was only 55 ± 6% ($P = 3.5 \times 10^{-4}$) of ATP1B1 expression remaining in KD1, 45 ± 6% ($P = 0.002$) in KD2 and 44 ± 22% ($P = 0.002$) in KD3 in comparison with time 0 ($n > 3$). These results show that the degradation rate is significantly different between WFS1 wild-type and depleted clones.

To elucidate how WFS1 stabilizes ATP6V1A and ATP1B1, we investigated the possibility that the WFS1 protein may protect these proteins from proteasomal degradation. We therefore inhibited the proteasome using the MG132 proteasome inhibitor. Control cells and two WFS1 protein depleted clones KD2 and KD3 were treated with increasing concentrations of MG132 (5, 10 and 20 μM) for 4 h, the cells harvested and samples resolved on sodium dodecyl sulfate–polyacrylamide gel electrophoresis (SDS–PAGE) gels (Fig. 6). Inhibition of the proteasome was demonstrated in all cell lines by the accumulation of ubiquitinylated proteins (global ubiquitinylation) by western blotting using an anti-ubiquitin antibody (Fig. 6A). The expression levels of ATP6V1A and ATP1B1 were tested at each of the treatment conditions in CL (Fig. 6B) and WFS1 depleted cells: KD2 (Fig. 6C) and KD3 (Fig. 6D). MG132 treatment did not restore the level of either of the subunits in WFS1 depleted cells to the level present in WFS1 positive CL and had no significant effect on their expression. Our results suggest that the WFS1 protein may be necessary for the stability of both ATP6V1A and ATP1B1, however do not support the hypothesis that the presence of WFS1 protects ATP6V1A and ATP1B1 from proteasomal degradation in neuronal cells.

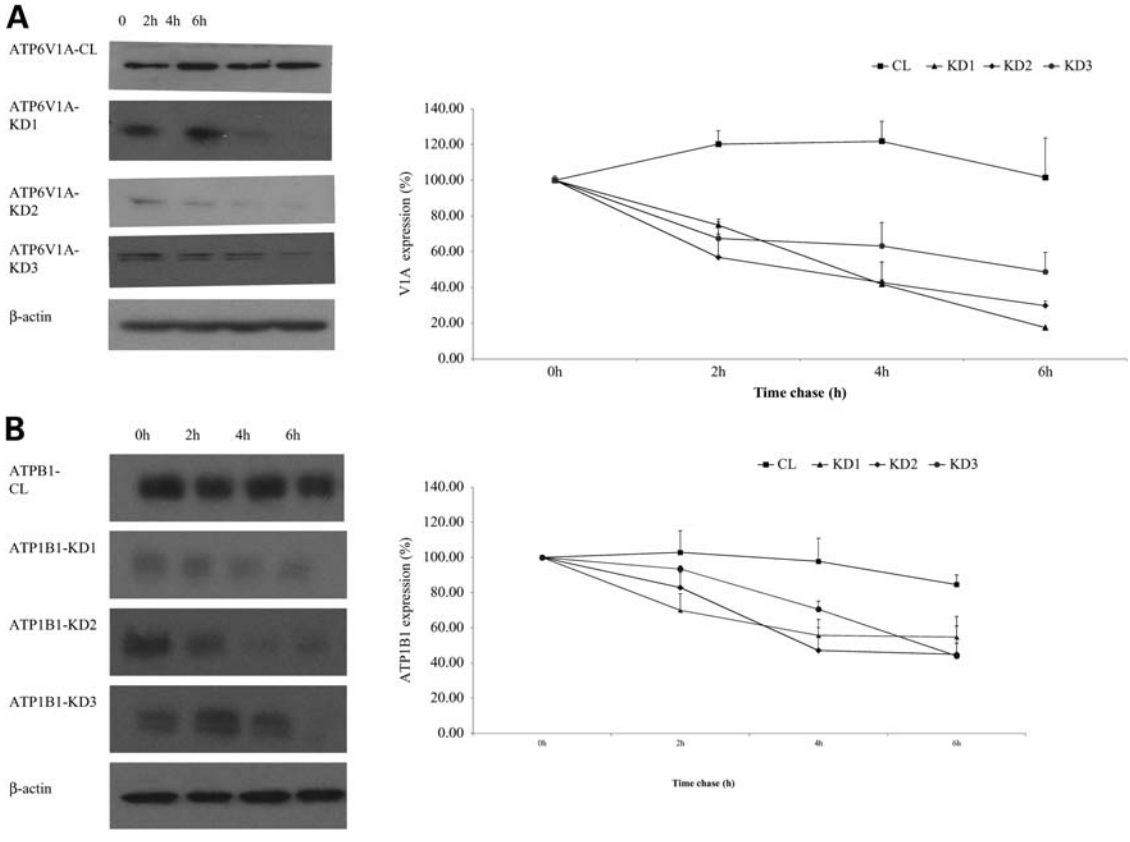

Figure 5. *WFS1* is necessary for ATP6V1A and ATP1B1 stability. CL, control; KD1, KD2 and KD3 stable depleted neuroblastoma clones. The expression of the β1 subunit of the sodium pump and the V1A subunit of the proton pump was at each time point normalized to the relevant β-actin. For the clarity of the figure, only one β-actin panel (for KD2) is chosen as representative for all clones. (**A**) Immunoblot with antibodies against the V1A subunit of the vesicular proton pump and β-actin showing the expression of ATP6V1A at 0, 2, 4 and 6 h after treatment with 50 μg/ml of CX- representative experiment. Quantitative comparison of the ATP6V1A degradation rate in WFS1 depleted stable clones. *t*-test: V1A levels at 2, 4 and 6 h after treatment versus time 0. CL: $P =$ NS, $n = 3$; KD1: $P < 0.001$, $n = 4$; KD2: $P < 0.05$, $n = 4$; KD3: $P < 0.05$, $n = 4$. (**B**) Immunoblot with antibodies against the β1 subunit of the sodium pump and β-actin showing the expression of ATP1B1 at 0, 2, 4 and 6 h after treatment with 50 μg/ml of CX—representative experiment in WFS1 depleted stable clones. Immunoblot quantification: *t*-test ATP1B1 levels at 2, 4 and 6 h after treatment versus time 0: CL $P =$ NS, $n = 4$; KD1 $P < 0.01$, $n = 4$; KD2 $P < 0.05$, $n = 4$; KD3 $P < 0.05$, $n = 3$.

WFS1 is involved in cell cycle regulation

Cell cycle kinetics and cell proliferation were investigated using High-Content Cytometry in the *WFS1* depleted neuroblastoma cells. Measured parameters indicated the percentage of cells in each phase of the cell cycle, population doubling time (PDT) and the length of each phase of the cell cycle. The cytometry was performed at 24 and 48 h time points, following an initial 24 h incubation (which allowed the cells to attach) and presented in Supplementary Material, Fig. S2 and Table 2. KD1 is a tetraploid cell line: the DNA content of the cells is double that seen in the CL and the other two cell lines (showing right shift in the cytometry histogram). Cell cycle kinetics data showed that in KD1, there were more cells in the G1 phase and fewer in the G2 phase; in KD2, there were fewer cells in the G1 phase and more in the G2 phase in comparison with CL cells at 24 and 48 h cell growth (Supplementary Material, Fig. S2B and Table 2). The percentages of cells in KD3 after 24 h of cell growth were significantly different from CL (fewer cells in the G1 phase and more cells in the G2 phase). However, at 48 h cell growth, this difference was not statistically significant. At 24 h, the differences between the CL and KD1 in the G1 and G2 phases were statistically significant ($P < 0.001$), KD2 versus CL ($P =$ NS) and KD3 versus CL ($P < 0.001$). At 48 h of cell growth, the differences between CL versus KD1 and KD2 were significant ($P < 0.001$) but the differences between CL and KD3 were not statistically significant ($P =$ NS).

The cell proliferation data presented in Supplementary Material, Fig. S2C and Table 2 show that the PDT was lower in KD2 in comparison with the other cell lines. The time spent in the G1 phase was longer in KD1 (39 h) and shorter in KD2 (14 h) in comparison with the CL (25 h). The differences between CL versus KD1 and KD2 were significant ($P < 0.001$), but the differences between CL and KD3 were not statistically significant ($P =$ NS). The time spent in the G2 phase was shorter in KD1 (16 h) and longer in KD2 (31 h) in comparison with the CL (Table 2). Overall, these results show that the KD1 line has a longer G1 phase whereas the KD2 line has an elongated G2 phase and a shorter PDT in comparison with the CL, but no significant differences were observed between CL and KD3.

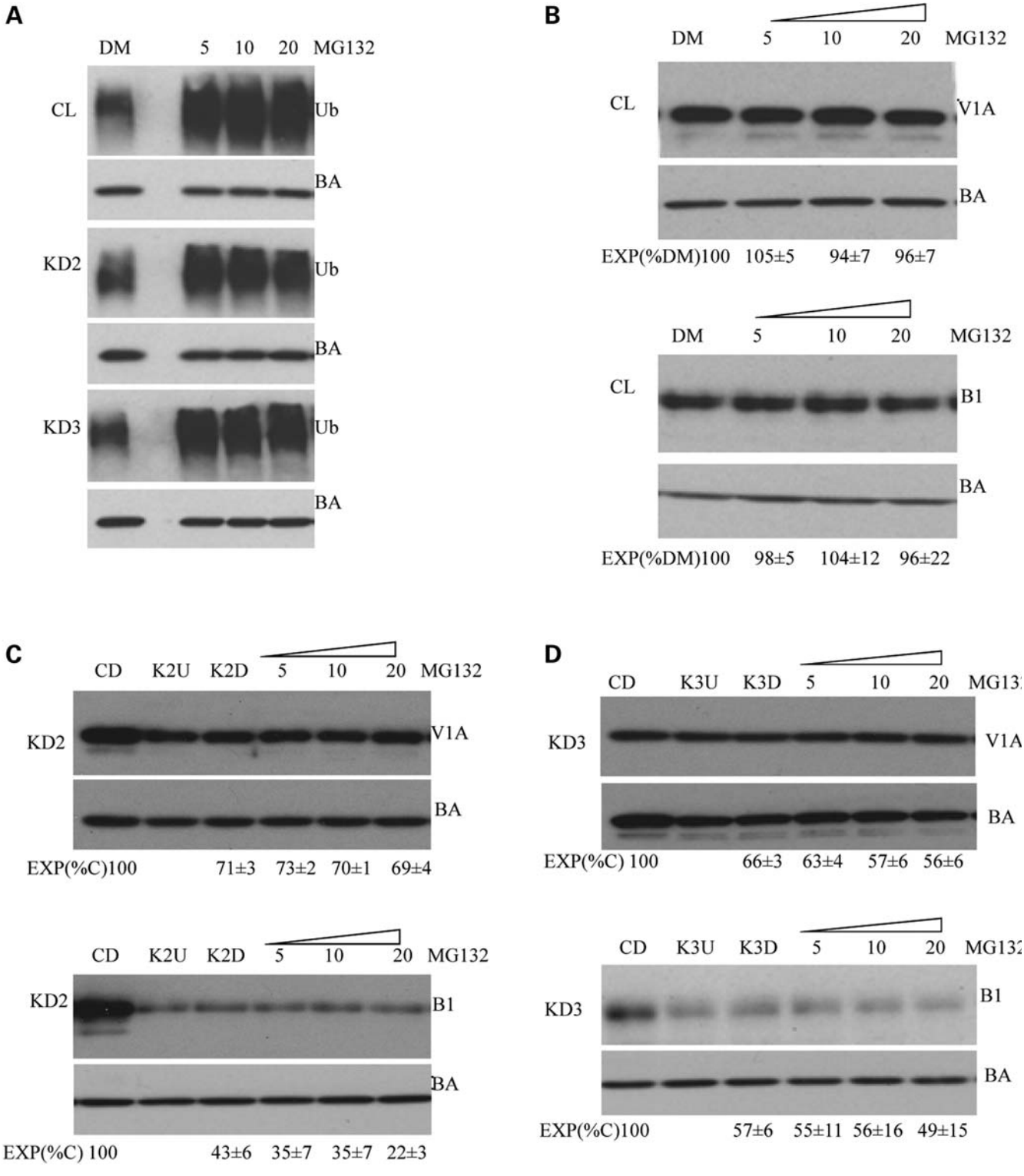

Figure 6. WFS1 does not protect ATP6V1A and ATP1B1 from proteasome-mediated degradation. CL, control; KD2 and KD3 stable depleted neuroblastoma clones. U, untreated; D, DMSO-treated samples, 5–20 increasing concentrations of MG132: 5–20 μM. (**A**) Proteasome inhibition: accumulation of ubiquitilated proteins after treatment for 4 h with 5, 10 and 20 μM MG132 proteasome inhibitor. Immunoblot with antibody detecting ubiquitinylated proteins (Ub) and β-actin (BA). (**B**) Inhibition of proteasome does not change the levels of ATP6V1A and ATP1B1 in WFS1 positive CL cells—representative immunoblot. Expression levels (EXP %DM) calculated as a percentage of DMSO-treated CL (assumed as 100%) are presented below immunoblots. *t*-test: MG132-treated versus DMSO-treated: V1A $P = 0.37$, 0.48 and 0.54; B1 $P = 0.69$, 0.71 and 0.76 for 5, 10 and 20 μM, respectively ($n = 3$, using independently treated extracts). (**C**) Inhibition of proteasome does not increase the levels of ATP6V1 and ATP1B1 in WFS1 depleted KD2 cells—representative immunoblot. Expression levels (EXP %C), calculated as a percentage of DMSO-treated CL (assumed as 100%) are presented below immunoblots. *t*-test: MG132-treated KD2 versus DMSO-treated KD2: V1A: $P = 0.70$, 0.60 and 0.68 and B1: $P = 0.34$, 0.30 and 0.02 for 5, 10 and 20 μM, respectively ($n \geq 3$ using independently treated extracts). K2U, untreated; K2D, DMSO treated. (**D**) Inhibition of proteasome does not increase the levels of ATP6V1 and ATP1B1 in WFS1 depleted KD3 cells: representative immunoblot. Expression levels (EXP %C) calculated as a percentage of DMSO-treated CL (assumed as 100%) are presented below immunoblot. *t*-test: MG132-treated KD3 versus DMSO-treated KD3; V1A, $P = 0.48$, 0.18 and 0.11; B1, $P = 0.87$, 0.96 and 0.63 for 5, 10 and 20 μM, respectively ($n \geq 3$ using independently treated extracts). K3U, untreated; K3D, DMSO treated.

Further, we evaluated whether the adenoviral overexpression of GRP78 affected the cell cycle kinetics. The data presented in Supplementary Material, Fig. S2D and Table 2 show that the number of G1 cells are significantly decreased in ad.BiP-infected cells in comparison with ad.GFP infection. An opposite image was observed in G2 cells to compensate. These data suggest that ad.BiP transfection normalizes the cell cycle kinetics by removing the cell cycle arrest from the G1 phase caused by ER stress.

We also evaluated whether the cell cycle effects of WFS1 were due to alterations in $p21^{cip}$ levels. We found that significant $p21^{cip}$ down-regulation was present in all three WFS1 depleted cell lines (Supplementary Material, Fig. S2E). The expression of $p21^{cip}$ was associated with the inhibition of progression through the G2 phase of the cell cycle and inhibition of apoptosis in all four cell lines. In the KD3 line (where $p21^{cip}$ expression was significantly lower), the cell cycle effect of the protein (namely inhibition of progression beyond G2) was also significantly less robust than in the other three cell lines [Supplementary Material, Fig. S2F; the ratio of % cells in the G2 phase that express $p21^{cip}$ versus cells that do not express $p21^{cip}$: KD3 (2), CL (3), KD1 (6) and KD2 (13); $P < 0.05$, KD1 versus CL], whereas the anti-apoptotic effect of $p21^{cip}$ was similar to that of the CL line [Supplementary Material, Fig. S2G; the ratio of % cells in apoptosis expressing $p21^{cip}$ versus cells not expressing $p21^{cip}$: KD3 (0.125), CL (0.1), KD1 (0.1) and KD2 (0.05)]. In the KD1 cell line, the cell cycle modulator effect of $p21^{cip}$ was significantly stronger than in CL [KD1 (6) and CL (3); $P < 0.05$], whereas in the KD2 line, both the cell cycle and anti-apoptotic effects of $p21^{cip}$ were significantly stronger than either CL or KD1 cell lines (Supplementary Material, Fig. S2F and G).

DISCUSSION

The WFS1 protein is thought to be a negative regulator of the ER stress response. The present study provides additional insights into its role in human neuronal cells. We observed the following: (i) WFS1 protein depletion in human neuronal cells results in raised ER stress response proteins, increased apoptosis and alterations in cell cycle kinetics; (ii) the WFS1 protein localizes to neurosecretory granules; (iii) the N-terminal (cytoplasmic) domain of the WFS1 protein interacts with the V1A subunit of H^+ V-ATPase; (iv) WFS1 protein depletion results in the reduced expression of the V1A subunit of H^+ V-ATPase; (v) the expression of this subunit and the β1 subunit of Na^+/K^+ ATPase are not affected by either the induction of ER stress in wild-type cells or the treatment of ER stress with the adenoviral overexpression of GRP78 (BiP) in WFS1 protein depleted cells; (vi) both pump subunits undergo more rapid degradation after CX treatment in WFS1 protein depleted cells, providing evidence that the WFS1 protein is necessary for the stability of these subunits; (vii) all WFS1 protein depleted cell lines showed variable cell cycle abnormalities; these were ameliorated by the adenoviral overexpression of GRP78 (BiP), suggesting that cell cycle dysregulation in WFS1 depleted cells are mediated via ER stress. These findings provide new insights into the mechanisms of neurodegeneration in WS.

We observed enhanced ER stress in both transiently and stably depleted cells, associated with the activation of the apoptotic pathway and impaired cell cycle progression, analogous to the ER stress-related diabetes described previously (7–10). We also observed HRD1 expression significantly increased in *WFS1* depleted neuroblastoma (Figure 1c), consistent with a previous study showing increased levels of HRD1 in *WFS1* depleeted MIN6 cells (9). We demonstrated the localization of the WFS1 protein to neurosecretory vesicles, similar to a recent report of localization to secretory granules in pancreatic β cells and reduced intra-vesicular acidification (17). Intragranular acidification depends on the operation of H^+ V-ATPase. We identified an interaction between the WFS1 protein and the V1A subunit of H^+ V-ATPase and demonstrated that the WFS1/V1A subunit interaction occurs with the WFS1 protein N-terminal domain (amino acids 1–321). WFS1 is an ER membrane protein with the C-terminal domain located in the ER lumen and the N-terminal domain in the cytoplasm. It is likely that the WFS1 protein assumes the same orientation across secretory vacuole membranes. The mature H^+ V-ATPase is located in the secretory vacuole membrane with the V1A subunit projecting into the cytoplasm. We therefore believe that the WFS1 protein/V1A interaction is likely to occur in the cytoplasm. H^+ V-ATPase has a 'ball-and-stalk' structure, with the V1 sector (including the V1A subunit) containing catalytic domains and the V0 sector constituting the proton pathway. Our data in conjunction with those of Hatanaka *et al*. (17) raise the intriguing possibility that WFS1 is required for the proper functioning of the vesicular proton pump in the acidification of vesicles, and that reduced acidification in the absence of WFS1 may affect the release of neurotransmitters from neurosecretory vesicles.

In nerve terminals, the vesicular proton pump has multiple functions including the acidification of synaptic vesicles essential for loading with neurotransmitters and normal vesicular trafficking. Subunits V1A and V1B mediate the hydrolysis of ATP at three reaction sites (23–25). Therefore, the reduced levels of the V1A subunit are likely to have functional consequences for the whole pump. We believe that the effects of WFS1 protein depletion are specific for the β1 and V1A subunits, as we saw no effects on the expression levels of other pump subunits.

The results of our CX experiments showed that both the ATP1B1 and ATP6V1A subunits were degraded more rapidly in the *WFS1* depleted cells in comparison with the CLs; this suggests that *WFS1* is necessary for their stability. However, no accumulation of either of the proteins was observed after the inhibition of the proteasome in WFS1 depleted cells. It is known that short-lived, cytosolic and misfolded proteins retained in the ER are degraded by proteasome, whereas the lysosome plays a role in the degradation of long-lived and transmembrane proteins. There is evidence for the degradation of Na^+/K^+ ATPase through both proteasomal and lysosomal pathways in kidney proximal tubule cells (26). It is therefore possible that the WFS1 protein protects these pump subunits from degradation by lysosomes or other, as yet unspecified, cellular proteases.

V-ATPases within secretory vesicles promote the activity of acid proteases that process prohormones to their mature forms (27). Thus, in pancreatic islet cells, the acidification of secretory vesicles is necessary for the processing of proinsulin to insulin (28). Second, V-ATPases provide the pH gradient or

membrane potential required to drive the coupled transport of small molecules, such as neurotransmitters (29). For example, in synaptic vesicles in glutaminergic neurons, the luminal positive membrane potential generated by the V-ATPase drives uptake of the negatively charged glutamate into the vesicle. In contrast, in synaptic vesicles containing norepinephrine, uptake of the transmitter utilizes the pH gradient via a proton coupled norepinephrine/H+ antiporter. In fact, virtually all neurotransmitter uptakes are directly energized by the V-ATPase. Acidification of secretory vesicles by V-ATPases thus plays an essential role in both neuronal and endocrine functions.

Yamada *et al*. reported cell cycle arrest and impaired cell cycle progression in *WFS1*-deficient islets (9). Our data on cell cycle kinetics showed that all three KD cell lines showed variable disturbances in cell cycle regulation. It is known that the cell cycle/apoptosis regulatory pathways are intricately interconnected consisting of different, sometimes opposite, signals (30, 31). It is therefore expected that variable WFS1 depletion, followed by different levels of acute ER stress and compensatory mechanisms (e.g. BiP) as well as varying effects of chronic ER stress (CHOP) will elicit very different patterns of expression for the (p53-dependent and p53-independent) cell cycle regulatory machinery. It is clear from Supplementary Material, Fig. S2D that the overexpression of BiP (in the adenoviral-infected cells) affects cell cycle regulation in all cell lines (including CL) and reduces the difference in cell cycle kinetics seen in the KD cells relative to the CL cells. Thus, ameliorating ER stress alone has a significant effect on cell cycle regulation.

The KD1 cell line became tetraploid after *WFS1* depletion with a marked accumulation of cells in the G1 phase of the cell cycle and the elongation of the G1 phase at the expense of the G2 phase. These changes may be an effect of WFS1 depletion and also suggest that the tetraploidy activates a G1 phase arrest associated with the high level of ER stress and apoptosis in these cells. The quantitative PCR (QPCR) results showed that the expression of CHOP was increased by 150% in this depleted cell line, and only 50% in KD2 and KD3; this could influence the cell cycle behaviour in comparison with KD2 and KD3. Adaptation via endopolyploidy can provide protection from stress and thus increase cell survival (32). The development of tetraploidy in KD1 therefore may be a result of the ER stress. In contrast to the KD1 cell line, the KD2 cell line showed an accumulation of cells in the G2 phase and an elongated G2 time (30 h, Table 2). The PDT of the cells in this knockdown was significantly lower than the CL. The KD2 line had normal diploid cells. Furthermore, the cell cycle and anti-apoptotic effects of $p21^{cip}$ were significantly stronger in KD2 than either in the CL or in KD1 cell lines. Overall, we found significant $p21^{cip}$ down-regulation in WFS1 depleted cells in comparison with the CLs; these findings are in contrast to the findings by Yamada *et al*. (9) who reported p53-independent increase in $P21^{cip1}$ in *WFS1* depleted cells associated with the inhibition of the G2 phase of the cell cycle. However, our findings are supported by studies (31), showing that chronic or severe unfolded protein response results in the down-regulation of $p21^{cip}$ and increased levels of CHOP.

In summary, we have shown that the WFS1 protein is a molecular partner of the V1A subunit of H^+ V-ATPase and co-localizes in secretory granules in neuroblastoma cells. The disruption of this interaction in WS provides a plausible link between the neurological and endocrine disorders seen in the syndrome. Our data suggest the possibility that the WFS1 protein is necessary for the stability of the V1A subunit independently of its role in ER stress.

MATERIALS AND METHODS

Cell culture and transfection

Stably depleted *WFS1* clones were prepared in human neuroblastoma cell line SK-NA-S using shRNA (Open Biosystems) and selected in medium containing puromycin at 2.5 μg/ml. The SK-N-AS cell line and stably depleted clones were grown in Dulbecco's modified Eagle's medium (DMEM; 4500 mg/l of L-glucose, L-glutamine and pyruvate, Invitrogen) supplemented with 10% fetal calf serum (FCS), penicillin (100 U/ml), streptomycin (100 μg/ml), glutamine and non-essential amino acids. The NT2 cells were grown in DMEM: F12 HAM media (Sigma) supplemented with 10% FCS, penicillin (100 U/ml), streptomycin (100 μg/ml) and L-glutamine. The HEK293 cells were grown in DMEM (as above) with 10% FCS and penicillin and streptomycin.

Transient gene silencing was performed using siRNA (Ambion) with two oligonucleotides (WFS1-57 and WFS1-58; targeting different regions of *WFS1*), at final concentration 8 nM. The transfection was performed using Interferin transfection reagent (Source Biosciences) according to the manufacturer's instructions. Cells were harvested for expression studies 72 h after transfection. The same procedure was used for SK-N-AS and NT2 cell lines.

Induction of ER stress with thapsigargin

Cells were grown in 10 cm dishes for 24 h to reach 80–90% confluency and starved for ~14 h in serum-free medium before they were treated with 1 μM thapsigargin in DMSO. The cells were harvested after 24 h of treatment in RIPA buffer. DMSO treatment was used as a negative CL.

Protein degradation assay

Cells were plated at 8×10^5 cells/well in a 6-well plate. After 24 h, the cells were treated with 50 μg/ml of CX (Sigma). The cells were harvested in RIPA buffer at 0, 2, 4 and 6 h after treatment and prepared as described for western blotting. The samples were resolved on SDS–PAGE gel. About 20 μg of protein extract was loaded per lane. CX toxicity was tested by High-Content Cytometry using a concentration range of 10–90 μg/ml. CX was dissolved in DMSO (1% final concentration in wells).

Proteasome inhibition assay

Cells were plated at 5×10^5cells/well in a 6-well plate. After 24 h, cells were treated with 5, 10 and 20 μM MG132 proteasome inhibitor for 4 h, harvested in RIPA buffer and prepared as

described for western blotting. The anti-ubiquitin rabbit monoclonal antibody (Millipore; detecting Lys48-linked ubiquitins) was used 1:1000 in 5% milk in TSBT (final concentration: 50 mM Tris–Cl, pH 7.5, 150 mM NaCl, 0.1% Tween-20).

Adenovirus amplification and purification

Samples of adenoviruses expressing either GFP (ad.GFP) or GRP78/BiP (ad.BiP) (33) were a kind gift from Professor Guy Rutter, Imperial College, London. The adenoviruses were amplified first on a small scale by infecting 60–70% confluent HEK293 cells in 25 cm tissue culture flasks with 1 μl of the obtained adenoviral sample. The cells were grown for several days until signs of infection were visible. At this stage, the cells were harvested together with the medium and half of this crude virus (~3 ml) was used to infect 75 cm flasks with 60–70% confluent HEK293 cells for large-scale amplification. The procedure was repeated for several rounds. Adenovirus was harvested by scraping and spinning down the cells at 1000*g* for 10 min at 4°C and 1/100 volume of *n*-butanol was added. The samples were incubated on ice for 1 h before being spun down at 1000*g*, for 10 min at 4°C. The supernatant was harvested and loaded onto a CsCl gradient. The virus was purified by CsCl banding. The titre of the virus was established using Adeno-X rapid titre kit (Clontech), as 1.7×10^{10} ifu/ml for both ad.GFP and ad.BiP.

Adenoviral transduction

Cells were seeded at 4×10^5 cells/well in a 6-well plate. After 24 h, the cells were infected with either ad.BiP or ad.GFP at multiplicity of infection (MOI) = 8.5. Approximately 16 h after the infection, the cells were washed once with PBS (phosphate-buffered saline) and fresh medium was added. The cells were harvested 48 h after the infection either in TRIzol for RNA measurements or in RIPA buffer for protein measurements.

Western blotting

The samples were harvested in either RIPA buffer (50 mM Tris, pH 8, 150 mM NaCl, 0.1% SDS, 1 mM ethylenediametetraacetic acid (EDTA), 0.5% deoxycholate, 1% Igepal and protease inhibitors cocktail, Roche) or Laemmli buffer (62.5 mM Tris, pH 6.3, 2% SDS, 25% glycerol, 5% β-mercapto ethanol and protease inhibitors). Cells were harvested by scraping, sonicated 2 × 10 s, centrifuged at 21910 *g* for 30 min at 4°C and the supernatant was collected. For the detection of ATF6, cells were harvested in ice-cold TNE buffer (50 mM Tris–HCl, pH 7.5, 150 mM NaCl, 1 mM EDTA, 1% Igepal and protease inhibitors cocktail) and lysed for 15 min on ice. The lysates were cleared by centrifugation at 12 000*g* for 20 min at 4°C. For the detection of ATF6, the antigen retrieval protocol was followed (15). The following primary antibodies were used: anti-WFS1 rabbit polyclonal (Proteintech Group, INC) 1:500; anti-BIP rabbit polyclonal (Abcam) 1:1000; anti-ATP1B1 mouse monoclonal (Sigma) 1:5000; anti-ATF6 rabbit polyclonal (Santa Cruz) 1:100; anti-HRD1 rabbit polyclonal (Abcam or Abgent) 1:100; anti-CHOP mouse monoclonal (Abcam and Santa Cruz) 1:100; anti-ATP6V1A rabbit polyclonal (Abcam) 1:500; anti-ATP6V1C1 rabbit polyclonal (Abcam) 1:2000; anti-ATP6V0D2 rabbit polyclonal (Abcam) 1:500; anti-cleaved caspase-3 rabbit monoclonal (Cell Signalling) 1:500 and anti-β actin (Sigma) 1:20 000. The secondary antibodies used were: anti-rabbit and anti-mouse (Dako) at a concentration of 1:20 000. The primary and secondary antibodies were prepared in 5% milk in PBS/Tween. Incubation with the primary antibody was performed overnight at 4°C while with the secondary antibody for 1 h at room temperature. Afterwards, the membrane was developed using ECL (electrochemiluminescence) or ECL plus kit (GE Healthcare). Quantitative analysis was performed by measuring integrated optical density using the program GeneTools.

cDNA cloning and generation of expression constructs

Cloning of full-length hWFS1 cDNA (amino acids 1–890), truncated WFS1 N terminus (amino acids 1–321) and truncated WFS1 C terminus (amino acids 652–890) in pCMV-Myc (Clontech) have been described in our previous study (16). The complete coding sequence of hATP6V1A (GeneBank accession number: NM_001690.3) was isolated from a neuroblastoma cDNA library by PCR using the following oligonucleotides: 5′-GCCGCGAATTCCATGGATTTTTCCAAGC-3′ and 5′-CG AGGTACCCTAATCTTCAAGGCTAC-3′ and was subsequently cloned into the *Eco*R1/*Kpn*I sites of the pFLAG-CMV-4 vector (Sigma). The sequence was then confirmed by DNA sequencing.

Transient transfection of HEK293 cells and IP

HEK293 cells were seeded at a density of 3×10^6/10 cm dish and after overnight incubation co-transfected with pCMV-Myc-WFS1 (full length, N-ter or C-ter)/pFLAG-CMV-ATP6V1A using the Turbofect transfection reagent (Fermentas) according to the manufacturer's instructions. For CLs, cells were co-transfected with pCMV-Myc-empty vector/pFLAG-CMV-ATP6V1A and pCMV-Myc-WFS1 (full length, N-ter or C-ter)/pFLAG-CMV-4 empty vector. After 48 h, cells were harvested in IP buffer (20 mM Tris–HCl, pH 7.4, 100 mM NaCl, 1% Triton X-100, 1 mM dithiothreitol, 1 mM phenylmethanesulfonylfluoride, 1 × protease inhibitors cocktail), incubated at 4°C for 30 min with end-to-end rotation and sonicated on ice for 30 s (10 s pulses with three intervals) and centrifuged at 9000*g* or 20 min at 4°C to remove cell debris.

For Co-IP in the overexpression system, 500 μg of protein lysate was incubated with either the WFS1 rabbit polyclonal antibody (Proteintech) or the rabbit polyclonal c-Myc antibody (Sigma) or the mouse monoclonal FLAG antibody overnight at 4°C with end-to-end rotation. Protein G sepharose beads (Sigma) were washed in IP buffer then added to the lysate–antibody complex and further incubated for 4 h. Beads were collected, washed twice in IP buffer with 150 mM NaCl, once in IP buffer with 500 mM NaCl and again in IP buffer with 150 mM NaCl. Bound proteins were then eluted in sample buffer.

To detect endogenous interaction, human neuroblastoma cells were harvested in IP buffer as described above. The

lysate (containing ~1 mg of protein) was precipitated with the rabbit polyclonal WFS1 antibody (Abcam). The mouse monoclonal FLAG antibody (Sigma) was used as a negative CL.

Real-time PCR and RNA isolation

RNA was isolated using TRIzol reagent (Invitrogen) according to the manufacturer's instructions. RNA was DNase treated for 30 min at 37°C (DNA-Free, Ambion) and converted to cDNA with High-Capacity cDNA Reverse Transcription Kit (Applied Biosystems). The following Taqman expression assays were used (Applied Biosystems): WFS1, Hs00903605_m1; BiP (endogenous, human), Hs99999174_m1; CHOP, Hs99999172_m1; spliced X-Box binding protein, Hs03929085_g1; GRP94 = Hs00427665_g1 and human beta actin, 4352935E. The expression of hamster BiP (expressed from adenovirus) was measured using Power SYBR Green mix (Applied Biosystems) with the following primers: hamster BiP 5′GGCCGCGTGGAGATCATA and 5′CACATACGAC GGCGTGAT and human β-actin 5′GGACTTCGAGCAA GAGATGG and 5′AGCACTGTGTTGGCGTACAG (Thermo Scientific). The expression of endogenous (human) BiP was measured using a set of primers specific to human BiP (Taqman expression assay). The plates were read using the BIO-RAD IQ5 machine.

Immunofluorescence microscopy

Wild-type SK-N-AS human neuroblastoma cell lines were plated on coverslips, fixed with 4% formaldehyde in PBS and permeabilized with 0.2% Triton X-100 in PBS. Cells were incubated overnight with primary antibodies and 1 h at room temperature with secondary antibodies. The cells were visualized and photographed with AXI-overt 100 M confocal image collection apparatus (Zeiss), using 65× lens. The following primary antibodies were used: sheep anti-N-terminal WFS1 1:100 (18); anti-ATP6V1A rabbit polyclonal (Abcam) 1:100; anti-VAMP1 rabbit polyclonal (Abcam) 1:100; anti-PDI mouse monoclonal (Stressgene) 1:50. Secondary antibodies used: Alexa 488 donkey anti-sheep 1:500 and Alexa 633 goat anti-mouse and anti-rabbit antibodies 1:1000 (Invitrogen).

Electron microscopy using pre-embedding immunostaining

Wild-type SK-N-AS human neuroblastoma cell lines were grown on plastic coverslips for 24 h. To reveal the subcellular distribution of Wolframin, cell cultures were cryoprotected in 30% sucrose (0.1 M phosphate buffer), freeze–thawed over liquid nitrogen and incubated in polyclonal rabbit anti-WFS1 (1:100) in Tris-buffer saline [0.05 M Tris-buffered saline (TBS)]. After intensive washing with TBS, cell cultures were incubated with goat anti-rabbit IgG coupled to 1 nm gold particles (Amersham, UK) diluted 1:50 overnight at 4°C. Then, cultures were washed and fixed for 10 min in 4% v/v formaldehyde solution (made up in PBS), washed three times 10 min in Enhancement Conditioning Solution (Aurion Immunoresearch, Wageningen, The Netherlands) and the gold particles were intensified with R-Gent silver intensification solution (Aurion). At the end of the immunogold reactions, cultures were treated with 1% OsO_4 (osmium tetroxide) for 15 min, dehydrated in graded ethanol (70% v/v ethanol containing 1% w/v uranyl acetate) and in propyleneoxide and embedded in Durcupan (Fluka Sigma-Aldrich). Regions of interest were re-embedded, sectioned serially in 50nm sections, collected on formvar-coated single slit copper grids, and counterstained with lead citrate. Electron micrographs were taken using a Tecnai Krios electron microscope equipped with digital camera.

High-Content Cytometry for cell cycle and apoptosis assays

About 5000 cells were seeded per well of a 96 well plate and incubated overnight. The next day, they were fixed with ice-cold 85% ethanol and stained with propidium iodide staining solution. The composition of the propidium iodide staining solution was 0.1% Triton X-100, 10 mg/ml propidium iodide, 100 mg/ml RNase A in PBS. The cells were incubated with the staining solution for 25 min at 37°C, and then DNA content based on the total fluorescence was measured with a High-Content Cytometer (Acumen). This allows rapid analysis of whole 96-well plates with resolution equivalent to a 20× microscope objective.

For $P21^{cip}$ staining, the cultured plate was first fixed with 1 × glyofix 100 μl/well for at least 2 h, followed by fixing with 100 μl/well ice-cold 85% ethanol for 30 min. The alcohol was aspirated and replaced with 100 μl/well blocking solution [5% bovine serum albumin in PBST (1:1000 Triton X)] and incubated for 30 min at room temperature. After aspirating the blocking solution, 50 μl/well primary antibody solution (monoclonal P21 Abcam, 1:1000 in PBST) was added and incubated overnight at 4°C and PBST was applied as a negative CL. The next day, the cells were washed by twice aspirating 200 μl/well PBST. Afterwards, 50 μl/well secondary antibody solution [anti-mouse IgG-fluorescein isothiocyanate (FITC), Abcam, 1:200 in PBST] was added, protecting the solutions and plates from light, and incubated overnight at +4°C. The next day, the cells were washed twice with 200 μl/well PBST and stained with propidium iodide solution as described above.

For ad.BiP infection experiments, adenoviral-treated cells were plated and grown for 24 h. After fixing, the plate was treated with the anti-BiP polyclonal rabbit antibody 1:800 (Abcam), and the secondary antibody anti-rabbit IgG-FITC (Abcam, 1:200 in PBST) was used in the same way as $p21^{cip}$ staining.

Statistical analysis

The data are presented as the mean ± SEM. Statistical significance was analysed by Student's two-sample *t*-test. A *P*-value of $P < 0.05$ was considered as statistically significant.

SUPPLEMENTARY MATERIAL

Supplementary Material is available at *HMG* online.

ACKNOWLEDGEMENTS

We are grateful to Professor Guy Rutter and Dr Gabriela Da Silva Xavier from Imperial College, London, for their kind gift of the GRP78/BIP adenoviral construct and advice on adenovirus; Dr Carmel McConville for the kind gift of the original SK-N-AS cell lines and Dr Shiao Chan for NT2 cell lines. Dr Chris Ricketts kindly helped with cell cultures. Dr Erzsebet M Rabai provided technical support for the high-content cytometry. Dr Ayrun Begum prepared the immune staining for the electron microscopy. Staff in Dr Peter Searle's laboratory, School of Cancer Sciences, University of Birmingham, helped with the CsCl banding. We are grateful for the involvement of patients in discussions of our research through the Wellcome Trust Clinical Research Facility, as part of the EURO-WABB project (www.euro-wabb.org).

Conflict of Interest statement. None declared.

FUNDING

This work was supported by the UK National Children's Charity Wellchild and a University of Birmingham PhD studentship funded by the MRC DTA (Doctoral Training Account); A.S. is supported by MRC (G1001235).

REFERENCES

1. Prusiner, S.B. (2001) Neurodegenerative diseases and prions. *N. Eng. J. Med.*, **344**, 1516–1526.
2. Barrett, T.G., Bundey, S.E. and Macleod, A.F. (1995) Neurodegeneration and diabetes—UK nationwide study of Wolfram (Didmoad) syndrome. *Lancet*, **346**, 1458–1463.
3. Genis, D., Davalos, A., Molins, A. and Ferrer, I. (1997) Wolfram syndrome: a neuropathological study. *Acta Neuropathol.*, **93**, 426–429.
4. Inoue, Y., Tanizawa, J., Wasson, J. and Behn, P. (1998) A gene encoding a transmembrane protein is mutated in patients with diabetes mellitus and optic atrophy (Wolfram syndrome). *Nat. Genet.*, **20**, 143–148.
5. Strom, T.M., Hortnagel, K., Hofmann, S., Gekeler, F., Scharfe, C., Rabl, W., Gerbitz, K.D. and Meitinger, T. (1998) Diabetes insipidus, diabetes mellitus, optic atrophy and deafness (DIDMOAD) caused by mutations in a novel gene (Wolframin) coding for a predicted transmembrane protein. *Hum. Mol. Genet.*, **7**, 2021–2028.
6. Takeda, K., Inoue, H., Tanizawa, Y., Matsuzaki, Y., Oba, J., Watanabe, Y., Shinoda, K. and Oka, Y. (2001) WFS1 (Wolfram syndrome 1) gene product: predominant subcellular localization to endoplasmic reticulum in cultured cells and neuronal expression in rat brain. *Hum. Mol. Genet.*, **10**, 477–484.
7. Fonseca, S.G., Fukuma, M., Lipson, K.L., Nguyen, L.X., Allen, J.R., Oka, Y. and Urano, F. (2005) WFS1 is a novel component of the unfolded protein response and maintains homeostasis of the endoplasmic reticulum in pancreatic beta-cells. *J. Biol. Chem.*, **280**, 39609–39615.
8. Riggs, A.C., Bernal-Mizrachi, E., Ohsugi, M., Wasson, J., Fatrai, S., Welling, C., Murray, J., Schmidt, R.E., Herrera, P.L. and Permutt, M.A. (2005) Mice conditionally lacking the Wolfram gene in pancreatic islet beta cells exhibit diabetes as a result of enhanced endoplasmic reticulum stress and apoptosis. *Diabetologia*, **48**, 2313–2321.
9. Yamada, T., Ishihara, H., Tamura, A., Takahashi, R., Yamaguchi, S., Takei, D., Tokita, A., Satake, C., Tashiro, F., Katagiri, H. *et al.* (2006) WFS1-deficiency increases endoplasmic reticulum stress, impairs cell cycle progression and triggers the apoptotic pathway specifically in pancreatic beta-cells. *Hum. Mol. Genet.*, **15**, 1600–1609.
10. Philbrook, C., Fritz, E. and Weiher, H. (2005) Expressional and functional studies of Wolframin, the gene function deficient in Wolfram syndrome, in mice and patient cells. *Exp. Gerontol.*, **40**, 671–678.
11. Luuk, H., Koks, S., Plaas, M., Hannibal, J., Rehfeld, J.F. and Vasar, E. (2008) Distribution of Wfs1 protein in the central nervous system of the mouse and its relation to clinical symptoms of the Wolfram syndrome. *J. Comp. Neurol.*, **509**, 642–660.
12. Swift, R.G., Sadler, D.B. and Swift, M. (1990) Psychiatric findings in Wolfram syndrome homozygotes. *Lancet*, **336**, 667–669.
13. Kõks, S., Planken, A., Luuk, H. and Vasar, E. (2002) Cat odour exposure increases the expression of Wolframin gene in the amygdaloid area of rat. *Neurosci. Lett.*, **322**, 116–120.
14. Luuk, H., Plaas, M., Raud, S., Innos, J., Sutt, S., Lasner, H., Abramov, U., Kurrikoff, K., Koks, S. and Vasar, E. (2009) Wfs1-deficient mice display impaired behavioural adaptation in stressful environment. *Behav. Brain Res.*, **198**, 334–345.
15. Fonseca, S.G., Ishigaki, S., Oslowski, C.M., Lu, S., Lipson, K.L., Ghosh, R., Hayashi, E., Ishihara, H., Oka, Y., Permutt, M.A. *et al.* (2010) Wolfram syndrome 1 gene negatively regulates ER stress signaling in rodent and human cells. *J. Clin. Invest.*, **120**, 744–755.
16. Zatyka, M., Ricketts, C., Xavier, G.D., Minton, J., Fenton, S., Hofmann-Thiel, S., Rutter, G.A. and Barrett, T.G. (2008) Sodium-potassium ATPase beta 1 subunit is a molecular partner of Wolframin, an endoplasmic reticulum protein involved in ER stress. *Hum. Mol. Genet.*, **17**, 190–200.
17. Hatanaka, M., Tanabe, K., Yanai, A., Ohta, Y., Kondo, M., Akiyama, M., Shinoda, K., Oka, Y. and Tanizawa, Y. (2011) Wolfram syndrome 1 gene (WFS1) product localizes to secretory granules and determines granule acidification in pancreatic β-cells. *Hum. Mol. Genet.*, **20**, 1274–1284.
18. Payne, W.P.B.a.S.L. (2005). High-content screening in oncology using fluorescence microplate cytometry. *Nat. Methods*, **2**, i–ii.
19. Short, B. (2010) The acid test of v-ATPase function. *J. Cell Biol.*, **189**, 773.
20. Futai, M., Oka, T., Sun-Wada, G., Moriyama, Y., Kanazawa, H. and Wada, Y. (2000) Luminal acidification of diverse organelles by V-ATPase in animal cells. *J. Exp. Biol.*, **203**, 107–116.
21. Ishihara, H., Takeda, S., Tamura, A., Takahashi, R., Yamaguchi, S., Takei, D., Yamada, T., Inoue, H., Soga, H., Katagiri, H. *et al.* (2004) Disruption of the WFS1 gene in mice causes progressive beta-cell loss and impaired stimulus-secretion coupling in insulin secretion. *Hum. Mol. Genet.*, **13**, 1159–1170.
22. Fu, H.Y., Minamino, T., Tsukamoto, O., Sawada, T., Asai, M., Kato, H., Asano, Y., Fujita, M., Takashima, S., Hori, M. *et al.* (2008) Overexpression of endoplasmic reticulum-resident chaperone attenuates cardiomyocyte deathinduced by proteosome inhibition. *Cardiovasc. Res.*, **79**, 600–610.
23. Tabares, L. and Betz, B. (2010) Multiple functions of the vesicular proton pump in nerve terminals. *Neuron*, **68**, 1020–1022.
24. Beyenbach, K.W. and Wieczorek, H. (2006) The V-type H+ ATPase: molecular structure and function, physiological roles and regulation. *J. Exp. Biol.*, **209**, 577–589.
25. Wieczorek, H., Beyenbach, K.W., Huss, M. and Vitavska, O. (2009) Vacuolar-type proton pumps in insect epithelia. *J. Exp. Biol.*, **212**, 1611–1619.
26. Thévenod, F., Friedmann, J.M., Katsen, A.D. and Hauser, I.A. (2000) Up-regulation of multidrug resistance P-glycoprotein via nuclear factor-κB activation protects kidney proximal tubule cells from cadmium- and reactive oxygen species-induced apoptosis. *J. Biol. Chem.*, **275**, 1887–1896.
27. Hinton, A., Sennoune, S.R., Bond, S., Fang, M., Reuveni, M., Sahagian, G.G., Jay, D., Martinez-Zaguilan, R. and Forgac, M. (2009) Function of a subunit isoforms of the V-ATPase in pH homeostasis and in vitro invasion of MDA-MB231 human breast cancer cells. *J. Biol. Chem.*, **284**, 16400–16408.
28. Sun-Wada, G.-H., Toyomura, T., Murata, Y., Yamamoto, A., Futai, M. and Wada, Y. (2006) The a3 isoform of V-ATPase regulates insulin secretion from pancreatic β-cells. *J. Cell Sci.*, **119**, 4531–4540.
29. Forgac, M. (2007) Vacuolar ATPases: rotary proton pumps in physiology and pathophysiology. *Nat. Rev. Mol. Cell Biol.*, **8**, 917–929.
30. Tabas, I. and Ron, D. (2011) Integrating the mechanisms of apoptosis induced by endoplasmic reticulum stress. *Nat. Cell Biol.*, **13**, 184–190.
31. Mihailidou, C., Papazian, I., Papavassiliou, A.G. and Kiaris, H. (2010) CHOP-dependent regulation of p21/waf1 during ER stress. *Cell. Physiol. Biochem.*, **25**, 761–766.
32. Lee, H.O., Davidson, J.M. and Duronio, R.J. (2009) Endoreplication: polyploidy with purpose. *Genes Dev.*, **23**, 2461–2477.
33. Fu, Y., Li, J. and Lee, A.S. (2007) GRP78/BiP inhibits endoplasmic reticulum BIK and protects human breast cancer cells against estrogen starvation-induced apoptosis. *Cancer Research*, **67**, 3734–3740.